Shape dependence of transmission, reflection, and absorption eigenvalue densities in disordered waveguides with dissipation

A. Yamilov, S. Petrenko, R. Sarma, and H. Cao

Phys. Rev. B **93**, 100201 — Published 3 March 2016

DOI: 10.1103/PhysRevB.93.100201

Shape-dependence of transmission, reflection and absorption eigenvalue densities in disordered waveguides with dissipation

A. Yamilov,[1,*] S. Petrenko,[1] R. Sarma,[2] and H. Cao[2,†]

[1] *Department of Physics, Missouri University of Science and Technology, Rolla, Missouri 65409, USA*
[2] *Department of Applied Physics, Yale University, New Haven, CT, 06520, USA*

(Dated: February 12, 2016)

The universal bimodal distribution of transmission eigenvalues in lossless diffusive systems underpins such celebrated phenomena as universal conductance fluctuations, quantum shot noise in condensed matter physics and enhanced transmission in optics and acoustics. Here, we show that in the presence of absorption, density of the transmission eigenvalues depends on the confinement geometry of scattering media. Furthermore, in an asymmetric waveguide, densities of the reflection and absorption eigenvalues also depend of the side from which the waves are incident. With increasing absorption, the density of absorption eigenvalues transforms from single-peak to double-peak function. Our findings open a new avenue for coherent control of wave transmission, reflection and absorption in random media.

PACS numbers: 42.25.Dd, 42.25.Bs, 72.15.-v

Mesoscopic electronic transport through a disordered conductor can be described by a $N \times N$ transmission matrix $\hat{t}$ which relates the amplitudes of N incoming and outgoing transverse modes [1]. Dimensionless conductance is $g = \langle \mathrm{Tr}\left(\hat{t}^\dagger \hat{t}\right)\rangle = \sum_n \langle \tau_n \rangle$, where τ_n are the eigenvalues of the matrix $\hat{t}^\dagger \hat{t}$ [2] and $\langle ... \rangle$ denotes ensemble average. Therefore, electron transport in a metallic wire can be viewed as parallel transmission over N orthogonal eigenchannels with individual transmissions of τ_n. Due to the mesoscopic correlations [3, 4], density of the transmission eigenvalues $\mathcal{D}(\tau)$ has a bimodal functional form [5–11] with peaks at $\tau \to 0$ and $\tau \to 1$ [12, 13]. This leads to e.g. universal conductance fluctuations [14, 15] and quantum shot noise [16, 17]. In Ref. [18], bimodal distribution was proven to be applicable to an arbitrary geometry of the conductor as long as the transport remains diffusive and free of dissipation.

The bimodal distribution obtained in the context of mesoscopic physics is also applicable to transport of classical waves in scattering media [19]. In optics, rapid development of wavefront shaping techniques has enabled experimental access to transmission eigenchannels [20] that allows control of total transmission [21–23] as well as focusing through turbid media [24–31]. Absorption, common in optics, breaks energy conservation and makes the density of transmission eigenvalues [32] as well as reflection [33–35] eigenvalues to depend on its strength. However, the questions of whether the geometry of the system could affect the eigenvalue density in dissipative systems and if so, how it would affect it, have not been addressed.

In this work we demonstrate that, unlike passive systems, the density of the transmission eigenvalues in absorbing disordered waveguides is geometry dependent, that is beyond predictions of the existing theory [32]. This opens possibility of tuning the functional form of the eigenvalue density by choosing the shape of the boundary. Furthermore, we show that dissipation makes a profound impact on the densities of reflection eigenvalues ρ and absorption eigenavlues α, that can even depend on which side of the waveguide is being illuminated in the case of asymmetric waveguide shape. This is attributed to the fact that reflection matrices for illumination from different sides are no longer related in the presence of dissipation. Above a certain absorption threshold, the density of absorption eigenvalues exhibits a qualitative transformation from a single-peak to a double-peak function. The additional peak at $\alpha \simeq 1$ enables a nearly complete absorption at any frequency with an appropriate input wavefront.

Transmission eigenvalues. We consider a variable width waveguide, schematically depicted in the inset of Fig. 1a, formed by reflecting boundaries at $y(z) = \pm W(z)/2$, where $W(z)$ is a smooth function of z. The leads on the left/right support N_L/N_R propagating modes. The transport through the disordered region $0 \le z \le L$ is described by a complex $N_R \times N_L$ matrix $\hat{t}$. For passive random media, density of the eigenvalues of matrix $\hat{t}^\dagger \hat{t}$ is $\mathcal{D}(\tau) = (g_p/2)\tau^{-1}(1-\tau)^{-1/2}$. In [36], we reproduce this result using the circuit theory of Ref. [18] with the dimensionless conductance given by $g_p[W(z)] = (k\ell/2)[\int_0^L W^{-1}(z)dz]^{-1}$, where $k = 2\pi/\lambda$ is the wavenumber, ℓ is the transport mean free path, and subscript p stands for "passive". For a waveguide with constant $W = N(\lambda/2)$ width we recover the well-known expression $g_p = (\pi/2)N\ell/L$ [37].

Figure 1a schematically depicts $\mathcal{D}(\tau)$ with three contributions from open, closed and evanescent eigenchannels. Open channels correspond to eigenvalues close to unity ($\tau_O < \tau < 1$) and closed channels correspond low transmission ($\tau_C < \tau < \tau_O$). Defining $\int_{\tau_O}^1 P(\tau)d\tau = g_p$ [12] gives $\tau_O \equiv [2e/(e^2+1)]^2 \simeq 0.42$. Together, open and closed channels are described by the bimodal distribution. The cutoff τ_C at the level of ballistic transmis-

sion [5, 37] is obtained by normalizing $\int_{\tau_C}^{1} \mathcal{D}(\tau)d\tau$ to the number of propagating channels $N_{min} = W_{min}/(\lambda/2)$, see Fig. 1a. In a waveguide with a constriction, there are $\min(N_L, N_R)$ transmission eigenchannels, among which $N_E = \min(N_L, N_R) - N_{min}$ are evanescent channels with intensity decaying on the scale of the wavelength inside the narrow portion of the waveguide and, therefore, $\tau \ll \tau_C$ for these channels [36]. This boundary separating evanescent and closed channels is exaggerated for illustration in Fig. 1a, as in practice $\tau_C \simeq 0$.

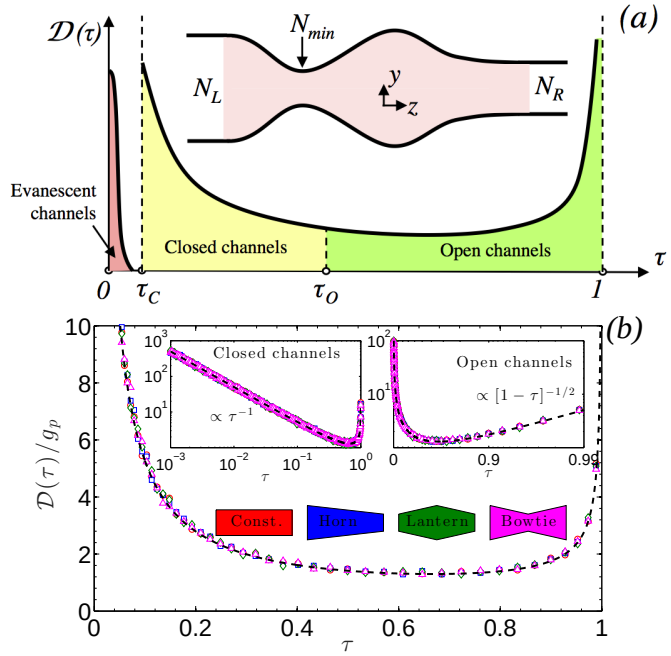

FIG. 1. (Color online) (a) Schematic illustration of density of the transmission eigenvalues $\mathcal{D}(\tau)$ in a passive disordered waveguide of varying width $W(z)$ drawn in the inset. It is made up of open ($\tau_O < \tau \leq 1$), closed ($\tau_C < \tau < \tau_O$) and evanescent ($\tau < \tau_C$) eigenchannels. (b) Normalized density of the transmission eigenvalues $\mathcal{D}(\tau)/g_p$ computed numerically for four passive waveguides shown. All data points fall onto the dashed line – the bimodal distribution. Two insets show that the bimodal distribution correctly describes both $\tau \to 0$ (closed channels) and $\tau \to 1$ (open channels) limits, regardless of the waveguide shape.

Applicability of the bimodal distribution for open and closed channels is confirmed in Fig. 1b. It shows $\mathcal{D}(\tau)/g_p$ computed numerically using Kwant simulation package [38] (see [36] for details) for four waveguides of different shape (drawn in the inset): rectangular waveguide of width $W = 273 \times (\lambda/2)$; horn waveguide of width linearly decreasing from $W_L = 400 \times (\lambda/2)$ to $W_R = 200 \times (\lambda/2)$; lantern waveguide of width linearly tapered from $W_M = 400 \times (\lambda/2)$ in the middle to $W_L = W_R = 200 \times (\lambda/2)$ at the two ends; and bowtie of width tapered from $W_L = W_R = 400 \times (\lambda/2)$ at the ends to $W_M = 200 \times (\lambda/2)$ in the middle. The conductance in the four systems is $g_p = 13.9,\ 14.2,\ 13.5$ and 13.9 respectively. The other system parameters are $L/\ell \simeq 31$, $k\ell \simeq 60$, $L/\lambda \simeq 300$. We accumulate ensembles of $\sim 5 \times 10^5$ eigenvalues so that their densities are free of noise over at least five decades of magnitude.

Fig. 1b clearly shows that the bimodal distribution, including the asymptotes for $\tau \to 0, 1$ in insets of Fig. 1b, describes open and closed eigenchannels in waveguides of different shapes without any fitting parameters. The nonuniversal contribution of evanescent channels to $\mathcal{D}(\tau \simeq 0)$ cannot be clearly distinguished from the peak of closed channels in the numerical data because $\tau_C \sim \exp(-L/\ell) \sim \exp(-31)$ cannot be resolved. Nevertheless, the evanescent channels can make up a substantial fraction of the total channels, e.g., in the bowtie waveguide, one half of the transmission eigenchannels are evanescent and have the vanishingly small values of τ.

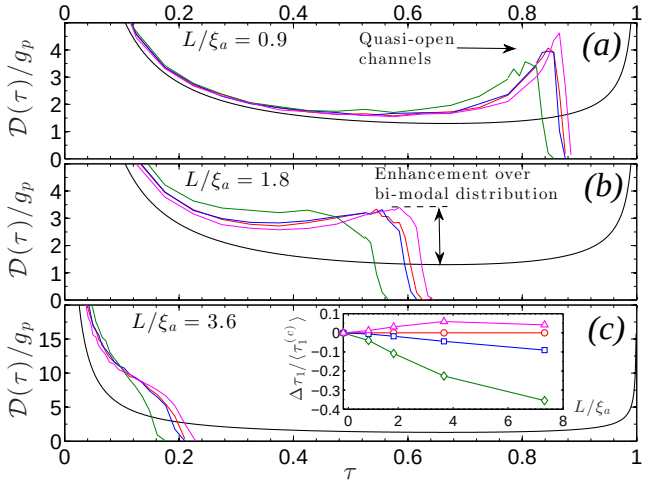

FIG. 2. (Color online) Density of the transmission eigenvalues $\mathcal{D}(\tau)/g_p$ in absorbing diffusive waveguides depends not only on the absorption strength but also on the confinement geometry. Four colored curves correspond to four waveguides with matched color in Fig. 1b. Absorption strength is $L/\xi_a = 0.9$ – (a), 1.8 – (b), and 3.6 – (c). The universal bimodal distribution of passive waveguides (solid line) is shown for reference. Inset of (c): normalized deviation of maximum transmission eigenvalue $\Delta\tau_1 = \langle\tau_1\rangle - \langle\tau_1^{(c)}\rangle$ in four waveguides of different shape from that in the rectangular waveguide $\langle\tau_1^{(c)}\rangle$, as a function of absorption L/ξ_a.

Absorption breaks flux conservation and time-reversal symmetry, leaving optical reciprocity the only constraint on the scattering matrix $\hat{S}$ of the system [39]. In [36] we show that it relates (in each realization of disorder) the transmission matrices for waves incident from the left $\hat{t}$ and right $\hat{t}'$ as $\hat{t}^T = \hat{t}'$, where superscript T denotes matrix transpose. This relationship signifies that even in the presence of absorption, $\hat{t}^\dagger\hat{t}$ and $\hat{t}'^\dagger\hat{t}'$ have the same set of non-zero eigenvalues.

Figures 2a-c show density of the transmission eigenvalues for waveguides of different shape with three values of absorption: $L/\xi_a = 0.9,\ 1.8$, and 3.6. $\xi_a = [\ell\ell_a/2]^{1/2}$

is the diffusive absorption length and ℓ_a is the ballistic absorption length. Common to all geometries, $\tau \simeq 1$ eigenvalues are attenuated so that the density no longer reaches unity. Instead, the maximum eigenvalue $\langle\tau_1\rangle < 1$. Open channels are redistributed throughout $\tau_C < \tau < \max(\tau_1)$ interval so that the eigenvalue density is consistently higher than that in passive systems. However, unlike the bimodal distribution for the passive systems, see Fig. 1b, $\mathcal{D}(\tau)$ *is no longer universal and exhibits a clear shape dependence.* The maximum transmission eigenvalue is lowest for the lantern geometry. Such behavior can be understood as the narrower openings and slanted walls of the lantern waveguide reduce the escape probability and increase the effective absorption, leading to smaller $\langle\tau_1\rangle$. In contrast, the situation is reversed in the bowtie waveguide, see Fig. 2. This structure has wider openings and, therefore, waves are more likely to escape without being strongly attenuated. The normalized deviation of the largest eigenvalue $\langle\tau_1\rangle$ in waveguides of different shapes from that in the rectangular waveguide, $\langle\tau_1^{(c)}\rangle$, is plotted in the inset of Fig. 2c. The deviation increases with absorption strength and can be either negative (horn, lantern) or positive (bowtie). However, at the largest value of absorption of $L/\xi_a \simeq 7.3$, the deviation is reduced in the bowtie waveguide, which can be understood as follows. For strong absorption $L \gg \xi_a$, short propagation paths dominate transport [29], so we expect the deviation to decrease in this limit because all geometries have the same length L. Such ballistic-like propagation is more favored due to the constriction in the bowtie waveguide, where this transition occurs first.

Reflection eigenvalues. In a passive system, the energy conservation and symmetry requirements make all non-zero eigenvalues of $\hat{t}^\dagger\hat{t}$, $\hat{I}-\hat{r}^\dagger\hat{r}$, $\hat{t}'^\dagger\hat{t}'$, $\hat{I}-\hat{r}'^\dagger\hat{r}'$ identical, where $\hat{r}$ ($\hat{r}'$) represents the reflection matrix for waves incident from left (right) end of the waveguide [36]. This leads to the bimodal distribution of the density of $1-\rho$ for both left and right reflection eigenvalues ρ and regardless of the shape of the waveguide. In an asymmetric waveguide with $N_L \neq N_R$ (we will assume $N_L > N_R$ without loss of generality), the $N_L \times N_L$ matrix $\hat{r}^\dagger\hat{r}$ also has $N_L - N_R$ eigenvalues with $\rho = 1$, giving the *perfectly reflecting eigenchannels* for light incident from the left (wider opening). Meanwhile, for waves incident from the right (narrower opening), there are no perfectly reflecting eigenchannels because $N_R \times N_R$ matrix $\hat{r}'^\dagger\hat{r}'$ has only N_R eigenvalues, all of which have corresponding transmission eigenvalues that are non-zero. The results of the numerical simulations in passive waveguides of different shape, c.f. Fig. 3, confirm that the density of both left/right reflection eigenvalues $\mathcal{D}(1-\rho)$ follows the universal bimodal distribution, which still holds in asymmetric waveguides as the perfectly reflecting eigenchannels only have a singular contribution at $\rho = 1$.

Due to absence of flux conservation in systems with absorption, the links between reflection and transmission matrices *and* between left/right reflection matrices are severed [36]. Consequently, in each disorder realization, the eigenvalues of $\hat{r}^\dagger\hat{r}$ and $\hat{r}'^\dagger\hat{r}'$ are not necessarily identical and they are no longer related to the transmission eigenvalues. Our numerical simulations confirm that the perfect reflecting channels are removed by absorption as *all* reflection eigenvalues become less than unity. Furthermore, in asymmetric waveguides ($N_L \neq N_R$), the densities of reflection eigenvalues differ for waves incident from left/right side of the waveguide, as shown in Figs. 3a,b for the horn geometry. Even for symmetric waveguides ($N_L = N_R$), $\mathcal{D}(\rho)$ is still clearly shape-dependent, as seen in Figs. 3a,b for the rectangular, lantern and bow-tie geometries: $\mathcal{D}(1-\rho)$ are distinctly different in $(1-\rho) \to 0$ limit while in the limit $(1-\rho) \to 1$ the difference is greatly reduced. The attenuation of reflection by absorption depends on how strong light is coupled into the absorbing waveguide, which can be controlled by the waveguide geometry. For example, the narrower opening and slanted

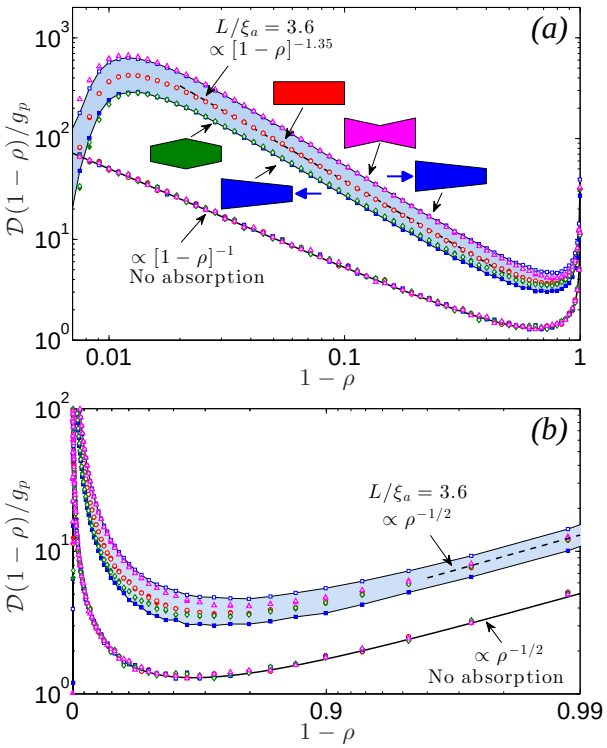

FIG. 3. (Color online) Density $\mathcal{D}(1-\rho)/g_p$ of the reflection eigenvalues ρ in diffusive waveguides of different shape with absorption ($L/\xi_a = 3.6$) and without absorption. Panels (a,b) show the power scaling behaviors at $(1-\rho) \to 0$ and 1 respectively. Without absorption all eigenvalue densities, regardless of the waveguide shape or input direction, fall onto the bimodal distribution – solid curve. In absorbing systems, $\mathcal{D}(1-\rho)/g_p$ obtained for waves incident from the left/right are shown with open/filled symbols. For all symmetric waveguides (rectangular, lantern, bowtie) with absorption, $N_L = N_R$, filled and open symbols coincide. For the asymmetric horn waveguide ($N_L \neq N_R$), a large disparity between left/right illumination is highlighted by shaded area.

sidewall of a lantern waveguide reduces the coupling of incident light, as compared to the bow-tie waveguide.

Figs. 3b shows that power exponent in $\mathcal{D}(1-\rho) \propto \rho^{-1}$ for $(1-\rho) \to 1$ is independent of the waveguide shape/input direction and it is the same as in a passive system. For $(1-\rho) \to (1-\rho_{max})$, we find that the power exponent in $\mathcal{D}(1-\rho) \propto (1-\rho)^{-1.35}$ has a weak shape dependence. The value 1.35 is smaller than 3/2 found in Refs. [33, 34] for $a = N\ell/\ell_a \gg 1$ in rectangular waveguides. We attribute the discrepancy to insufficiently large value of $a = 1.9$ for the case shown in Fig. 3a.

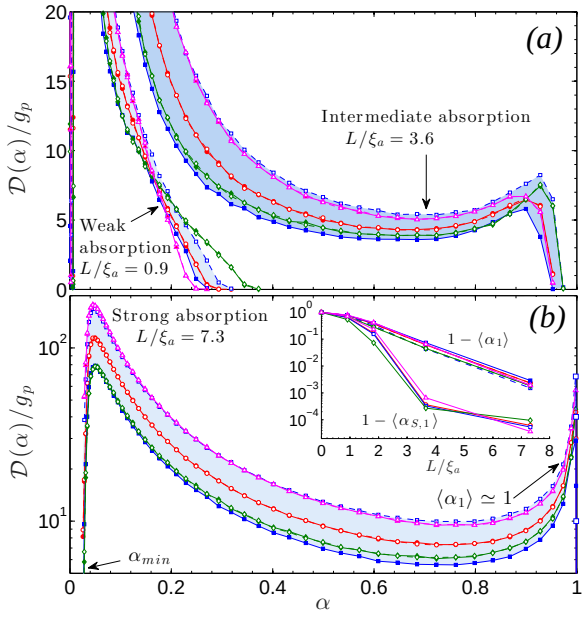

FIG. 4. (Color online) Density $\mathcal{D}(\alpha)$ of absorption eigenvalues α in disordered waveguides of different shape, under on-sided illumination, evolves from one peak function at weak absorption (the ensemble-averaged maximum absorption eigenvalue $\langle\alpha_1\rangle \ll 1$) to double peak function at intermediate absorption ($\langle\alpha_1\rangle \lesssim 1$) in panel a, and the second peak moves to $\alpha \simeq 1$ at strong absorption ($\langle\alpha_1\rangle \simeq 1$) in panel b. Symbol notations are the same as in Fig. 3. In all cases the normalized density of absorption eigenvalues exhibits strong dependence on the shape of the waveguide, and for asymmetric (horn) waveguide also on the input direction. The inset in panel (b) plots the ensemble-averaged maximum absorption eigenvalue $\langle\alpha_1\rangle$ vs. the absorption strength L/ξ_a. For comparison, the maximum absorption eigenvalue $\langle\alpha_{S,1}\rangle$ for two-sided illumination are also shown.

Absorption eigenvalues. In a dissipative system, the non-unitary part of the scattering matrix $\hat{I} - \hat{S}^\dagger\hat{S} \equiv \hat{A}_S$ accounts for absorption [40] and its largest eigenvalue $\alpha_{S,1}$ tells the maximum absorption that can be achieved by shaping the input wavefront [30]. This requires controlling all modes incident onto both sides of the waveguide. However, more common in experiments is only one side of the system illuminated. In such case the matrix $\hat{A} = \hat{I} - \hat{r}^\dagger\hat{r} - \hat{t}^\dagger\hat{t}$ describes the absorption of input light. Its largest eigenvalue α_1 determines the maximum absorption in a given system when only one side is accessible. Similar to density of the reflection eigenvalues, $\mathcal{D}(\alpha)$ depends on the shape of the waveguide and the input direction, c.f. Fig. 4a,b. Common to all geometries, the functional form of $\mathcal{D}(\alpha)$ undergoes a qualitative change with an increase of absorption strength. At weak absorption, the eigenvalue density monotonously decreases toward zero with an increase of α, c.f. Fig. 4a. At the increased absorption, the density develops the second maximum at $\alpha \simeq 1$. Even in this regime, there exists an upper bound, which approaches unity exponentially, c.f. inset of 4b. A coherent perfect absorber proposed in Ref. [41] achieves 100% absorption but requires full control of incident wavefront and a specific amount of absorption. In contrast, we show that at any frequency and with any absorption (above a certain threshold) the maximum achievable absorption with one-sided excitation α_1 can be close to unity. Moreover, with the left end of the waveguide being illuminated, for example, we can achieve nearly perfect absorption by controlling a fraction $N_L/(N_L+N_R)$ of all input channels, that can be small in e.g. a horn waveguide with $N_L < N_R$.

We note that absorption dependence of the maximum eigenvalue $\langle\alpha_1\rangle$ for one-sided illumination is qualitatively different from $\langle\alpha_{S,1}\rangle$ for two-sided illumination, c.f. inset in Fig. 4b. The former approaches unity exponentially, $1-\langle\alpha_1\rangle \propto \exp[-L/\xi_a]$. In contrast, excitation from both sides results in a sharp transition at $L/\xi_a \sim 3$, above which strong enhancement of absorption [30] with $\langle\alpha_{S,1}\rangle \simeq 1$ becomes possible. The critical value of absorption can be estimated by comparing the diffusion time without absorption $L^2/D\pi^2$ to the absorption time $t_a = \xi_a^2/D$, where D is the diffusion coefficient. Equating these two characteristic time scales results in $L/\xi_a = \pi$ which agrees with Fig. 4b. This offers an absorption analogy with diffusive random laser [42–44] where exactly the same amount of gain corresponds to the lasing threshold, giving *output* to all sides.

Conclusions. We believe our results will have profound implications for coherent control of wave transmission, reflection and absorption in random media [20, 45]. The ability to modify the eigenvalue densities will greatly enhance the capability of coherent control, with applications to imaging through opaque media and targeted deposition of energy inside turbid media. Furthermore, nanophotonic waveguides with various geometries can be readily made with current nanofabrication techniques [46], and the control of light transmission or reflection by shaping the incident wavefront will enable novel functionalities for photonic applications.

Acknowledgments. We thank A. D. Stone, P. Brouwer, C. W. J. Beenakker for stimulating discussions and B. van Heck for technical help with Kwant simulation package. This work is supported by the National Science Foundation under Grants No. DMR-1205307 and DMR-1205223.

* yamilov@mst.edu
† hui.cao@yale.edu

[1] R. Landauer, Phil. Mag. , 863 (1970).
[2] D. S. Fisher and P. A. Lee, Phys. Rev. B **23**, 6851 (1981).
[3] R. Berkovits and S. Feng, Physics Reports **238**, 135 (1994).
[4] M. C. van Rossum and T. M. Nieuwenhuizen, Rev. Mod. Phys. **71**, 313 (1999).
[5] O. N. Dorokhov, Solid State Comm. **51**, 381 (1984).
[6] J. L. Pichard and G. André, Europhys. Lett. **2**, 477 (1986).
[7] K. A. Muttalib, J. L. Pichard, and A. D. Stone, Phys. Rev. Lett. **59**, 2475 (1987).
[8] P. A. Mello and J. L. Pichard, Phys. Rev. B **40**, 5276 (1989).
[9] C. W. J. Beenakker and B. Rajaei, Phys. Rev. B **49**, 7499 (1994).
[10] A. Altland, A. Kamenev, and C. Tian, Phys. Rev. Lett. **95**, 206601 (2005).
[11] B. Gérardin, J. Laurent, A. Derode, C. Prada, and A. Aubry, Phys. Rev. Lett. **113**, 173901 (2014).
[12] Y. Imry, Europhys. Lett. **1**, 249 (1986).
[13] J. B. Pendry, A. MacKinnon, and P. J. Roberts, Proc. Math. Phys. Sc. **437**, 67 (1992).
[14] P. A. Lee and A. D. Stone, Phys. Rev. Lett. **55**, 1622 (1985).
[15] B. L. Altshuler, P. A. Lee, and R. A. Webb, eds., *Mesoscopic Phenomena in Solids* (North Holland, Amsterdam, 1991).
[16] C. W. J. Beenakker and M. Büttiker, Phys. Rev. B **46**, 1889 (1992).
[17] B. L. Altshuler, L. S. Levitov, and A. Y. Yakovets, JETP Lett. **59** (1994).
[18] Y. V. Nazarov, Phys. Rev. Lett. **73**, 134 (1994).
[19] E. Akkermans and G. Montambaux, *Mesoscopic Physics of Electrons and Photons* (Cambridge University Press, Cambridge, UK, 2007).
[20] P. A. Mosk, A. Lagendijk, G. Lerosey, and M. Fink, Nat. Photon. **6**, 283 (2012).
[21] M. Kim, Y. Choi, C. Yoon, W. Choi, J. Kim, Q. H. Park, and W. Choi, Nat. Photon. **6**, 581 (2012).
[22] H. Yu, T. R. Hillman, W. Choi, J. O. Lee, M. S. Feld, R. R. Dasari, and Y. K. Park, Phys. Rev. Lett. **111**, 153902 (2013).
[23] S. M. Popoff, A. Goetschy, S. F. Liew, A. D. Stone, and H. Cao, Phys. Rev. Lett. **112**, 133903 (2014).
[24] I. M. Vellekoop and A. P. Mosk, Phys. Rev. Let. **101**, 120601 (2008).
[25] Z. Shi and A. Z. Genack, Phys. Rev. Lett. **108**, 043901 (2012).
[26] S. M. Popoff, G. Lerosey, R. Carminati, M. Fink, A. C. Boccara, and S. Gigan, Phys. Rev. Lett. **104**, 100601 (2010).
[27] T. Kohlgraf-Owens and A. Dogariu, Opt. Lett. **35**, 2236 (2010).
[28] O. Katz, E. Small, Y. Bromberg, and Y. Silberberg, Nat. Photon. **5**, 372 (2011).
[29] S. F. Liew, S. M. Popoff, A. P. Mosk, W. L. Vos, and H. Cao, Phys. Rev. B **89**, 224202 (2014), 10.1103/PhysRevB.89.224202.
[30] Y. D. Chong and A. D. Stone, Phys. Rev. Lett. **107**, 163901 (2011).
[31] X. Cheng and A. Z. Genack, Opt. Lett. **39**, 6324 (2014).
[32] P. W. Brouwer, Phys. Rev. B **57**, 10526 (1998).
[33] N. A. Bruce and J. T. Chalker, J. Phys. A **29**, 3761 (1996).
[34] C. W. J. Beenakker, J. C. J. Paasschens, and P. W. Brouwer, Phys. Rev. Lett. **76**, 1368 (1996).
[35] A. Goetschy and A. D. Stone, Phys. Rev. Lett. **111**, 063901 (2013).
[36] "Supplementary information,".
[37] C. W. Beenakker, Rev. Mod. Phys. **69**, 731 (1997).
[38] C. W. Groth, M. Wimmer, A. R. Akhmerov, and X. Waintal, New J. Phys. **16**, 063065 (2014).
[39] R. Carminati, J. J. Sáenz, J.-J. Greffet, and M. Nieto-Vesperinas, Phys. Rev. A **62**, 012712 (2000).
[40] C. W. J. Beenakker, Phys. Rev. Lett. **81**, 1829 (1998).
[41] Y. D. Chong, L. Ge, H. Cao, and A. D. Stone, Phys. Rev. Lett. **105**, 053901 (2010).
[42] N. M. Lawandy, R. M. Balachandran, A. S. L. Gomes, and E. Sauvain, Nature **368**, 436 (1994).
[43] H. Cao, in *Progress in optics*, Vol. 45, edited by E. Wolf (North Holland, 2003).
[44] A. Yamilov, S. H. Chang, A. Burin, A. Taflove, and H. Cao, Phys. Rev. B **71**, 092201 (2005).
[45] H. Yu, J. Park, K. Lee, J. Yoon, K. Kim, S. Lee, and Y. K. Park, Curr. Appl. Phys. **15**, 632 (2015).
[46] R. Sarma, T. Golubev, A. Yamilov, and H. Cao, Appl. Phys. Lett. **105**, 041104 (2014).